AD-A179 698 SIMULTANEOUS SMM FLAT CRYSTAL SPECTROMETER AND VERY LARGE ARRAY OBSERVATI..(U) TUFTS UNIV MEDFORD MA DEPT OF PHYSICS AND ASTRONOMY K R LANG ET AL. 1986 1/1

UNCLASSIFIED N00014-86-K-0068 F/G 3/2 NL

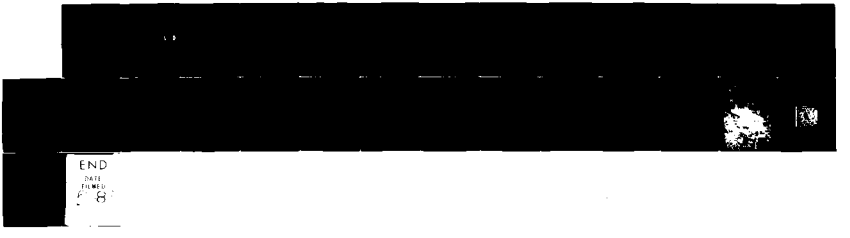

END

DATE FILMED

F 8

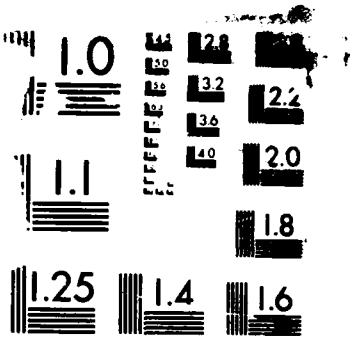
1.0
1.1
1.25
1.4
1.6
1.8
2.0
2.2
2.8
3.2
3.6
4.0

DTIC FILE COPY

AD-A179 698

L. SIMULTANEOUS SMM FLAT CRYSTAL SPECTROMETER AND VERY LARGE ARRAY OBSERVATIONS OF SOLAR ACTIVE REGIONS

Kenneth R. Lang and Robert F. Willson
Department of Physics and Astronomy
Tufts University
Medford, Massachusetts

and

Kermit L. Smith and Keith T. Strong
Lockheed Palo Alto Research Laboratory
Palo Alto, California

DTIC
ELECTE
APR 27 1987
S D
D

AFOSR-83-0019
N00014-86-K-0068

DISTRIBUTION STATEMENT A
Approved for public release;
Distribution Unlimited

ABSTRACT

We compare high-resolution images of the quiescent emission from two solar active regions at 20 cm (VLA) and soft X-ray (SMM-FCS) wavelengths. There are regions where the X-ray coronal loops have been completely imaged at 20 cm wavelength. In other regions, the X-ray radiation was detected without detectable 20 cm radiation, and vice versa. The X-ray data were used to infer average electron temperatures T_e of about 3,000,000 K and average electron densities of about 2.5×10^9 per cc for the X-ray emitting plasma in the two active regions. The thermal bremsstrahlung of the X-ray emitting plasma is probably optically thin at 20 cm wavelength. Although the 20-cm brightness temperatures T_B were always less than T_e, suggesting optically thin layers, the thermal gyroresonance radiation from the X-ray emitting plasma ought to be optically thick at 20 cm wavelength. The low T_B can be explained if a higher, cooler plasma covers the hotter X-ray emitting plasma. Thermal gyroresonance radiation must account for the intense 20-cm radiation near and above sunspots where no X-ray radiation is detected. The potential of 20-cm (VLA) and soft X-ray (SMM-FCS) comparisons is discussed.

Accesion For	
NTIS CRA&I	☑
DTIC TAB	☐
Unannounced	☐
Justification	
By	
Distribution/	
Availability Codes	
Dist	Avail and/or Special
A-1	

QUALITY INSPECTED 2

I. INTRODUCTION

High-resolution observations with X-ray telescopes orbiting above the atmosphere have transformed our understanding of the solar corona. The corona is now viewed as a highly inhomogeneous distribution of closed magnetic loops that are anchored in the Sun, and open magnetic fields that extend out into interplanetary space [see Vaiana and Rosner (1978) for a review]. The hot, dense plasma that is trapped within coronal loops gives rise to intense X-ray radiation, and observations of X-ray spectral lines can be used to infer the electron temperature, electron density, and emission measure of this plasma.

The development of aperture synthesis telescopes like the Very Large Array (VLA) has permitted ground-based microwave observations of the solar corona with angular resolutions that are comparable to those of X-ray telescopes. The high-resolution microwave observations can uniquely specify the strength and structure of the coronal magnetic field. VLA synthesis maps of the total intensity, I, describe the two-dimensional distribution of source brightness, whereas synthesis maps of circular polarization, or Stokes parameter V, describe the two-dimensional structure of the longitudinal magnetic field [see Kundu and Lang (1985) for a review].

The microwave brightness temperature, T_B, of the quiescent, or non-flaring, corona is nearly equal to the coronal electron temperature, T_e, with $T_B \approx T_e \approx 10^6$ K. This suggests that the quiescent microwave emission is thermal. However, there are two possible thermal radiation mechanisms. They are thermal bremsstrahlung, or free-free emission, and thermal gyroresonance radiation, or cyclotron emission. In contrast, the quiescent X-ray emission of the solar corona is mainly due to thermal bremsstrahlung.

To identify the dominant thermal radiation mechanism at microwave wavelengths, one needs to know the electron temperature, the electron density

and the magnetic field strength, as well as the thickness of the radiating layer, the scale length of the magnetic field, and the angle between the line of sight and the magnetic field. Thermal gyroresonance will generally dominate radiation at centimeter wavelengths when the electron density is relatively low and the magnetic field is strong.

Early evidence for thermal gyroresonance radiation at coronal levels above sunspots was provided by comparison of the soft X-ray and centimeter-wavelength radiation of active regions (Kundu, Schmahl and Gerassimenko 1980; Pallavicini, Sakurai and Vaiana 1981). Bright microwave radiation was found in the strong magnetic fields above sunspots, but the X-ray observations indicated a relatively low electron density in these regions. This meant that the high microwave brightness temperatures above sunspots could not be due to thermal bremsstrahlung, but it could be explained by thermal gyroresonant radiation at the second or third harmonic of the gyrofrequency.

These early low-resolution comparisons were fully confirmed when high-resolution synthesis maps at 6 cm wavelength were compared with simultaneous soft X-ray images obtained with the X-ray Polychromator (XRP) aboard the Solar Maximum Mission (SMM) satellite (Chiuderi-Drago et al. 1982; Schmahl et al. 1982; Shibasaki et al. 1983; Strong, Alissandrakis and Kundu 1984). Soft X-ray spectral lines were used to determine the electron temperature and electron density of the X-ray emitting plasma that coincided with the sunspot-associated 6 cm sources. These parameters were then used to compute the bremsstrahlung brightness temperature at 6 cm. Because the computed value was much less than the observed brightness temperature, additional 6 cm opacity due to gyroresonance absorption above sunspots was required.

Thermal gyroresonance radiation at 6 cm in coronal regions above sunspots was additionally confirmed by the detection of circularly polarized ring-shaped or

horseshoe shaped structures (Alissandrakis and Kundu 1982; Lang and Willson 1982). The highly polarized (up to 100 percent) structures were predicted by the theory of cyclotron radiation in the curved magnetic fields above sunspots (Gel'freikh and Lubyshev 1979). Depressions in the 6-cm brightness temperature above sunspot umbrae have been attributed to cool material in these regions (Strong, Alissandrakis and Kundu 1984).

What about the microwave counterpart of the intense X-ray sources? The brightest 6-cm sources are not usually associated with the brightest X-ray sources, and the detailed correspondence between the radiation at the two wave-lengths is poor (Schmahl et al. 1982; Webb et al. 1983). However, this result is not particularly surprising. It would be expected if the dominant radiation mechanisms are different in the two wavelength domains. Thermal bremsstrahlung is often too optically thin to be detected at 6-cm wavelength where gyroresonant radiation dominates. Different structures are observed at the two wavelengths because 6 cm gyroresonance absorption occurs in the strong magnetic fields above sunspots while the X-ray emission originates in coronal loops that stretch between sunspots of opposite magnetic polarity.

The hot temperatures, slow evolution, and long lifetime of X-ray coronal loops make them ideal candidates for aperture synthesis techniques. Of course, low-lying loops have occasionally been detected at 6 cm (Strong, Allisandrakis and Kundu 1984, Webb et al. 1986), but radiation at this wavelength originates at relatively low heights and is usually dominated by gyroresonance absorption. Higher levels are observed at 20 cm wavelength where the thermal bremsstrahlung of coronal loops can become optically thick. In fact, when VLA observations were extended to the longer 20 cm wavelength, quiescent loop-like coronal features were discovered (Lang, Willson and Rayrole 1982).

The coronal loops seen at 20 cm strongly resemble their X-ray counterparts (Lang and Willson 1983, 1984). They have million-degree temperatures and stretch across

regions of opposite magnetic polarity in the underlying photosphere. The size and shape of the loops observed at 20 cm are also similar to those of arcades of X-ray coronal loops, with linear extents $L \approx 10^9$ to 10^{10} cm. In addition, the electron temperature and electron density inferred from X-ray observations of other loops are consistent with the idea that the microwave loops are due to thermal radiation from the X-ray emitting plasma. All of these similarities suggest that the microwave counterpart of X-ray coronal loops can be observed in VLA synthesis maps at 20 cm.

Numerous authors have now identified elongated, loop-like features at 20 cm with coronal loops, but the exact radiation mechanism for the 20-cm emission remains controversial. Many authors have attributed this radiation to the optically-thick thermal bremsstrahlung of a hot, dense plasma trapped within coronal magnetic loops that connect with underlying sunspots (Lang, Willson and Rayrole 1982; Dulk and Gary 1983; Lang, Willson and Gaizauskas 1983; Lang and Willson 1983, 1984; Gary and Hurford 1986; Holman 1986). Others reason that optically thick thermal gyroresonance radiation may dominate the 20-cm emission of coronal loops (McConnell and Kundu 1983; Shevgaonkar and Kundu 1984, Lang et al. 1986). Both radiation mechanisms could play a role, with gyroresonance radiation becoming important at relatively high brightness temperatures or relatively low electron densities.

One can distinguish between the two thermal radiation mechanisms for the 20-cm emission from the coronal loops if the VLA synthesis maps are compared with simultaneous X-ray images. This has only been done twice. Chiuderi-Drago et al. (1982) used X-ray spectral lines from the SMM-FCS to infer the electron temperature and emission measure of the X-ray emitting plasma, concluding that one 20-cm source is the optically thin bremsstrahlung of this plasma. The angular extent of the X-ray source was comparable to that of the 20-cm one, but the observations at both wavelengths were of relatively poor angular resolution. Another sunspot-associated

20-cm source had to be attributed to gyroresonance radiation, for there was no detectable X-ray radiation from this region. Webb et al. (1986) used X-ray data taken during a recent rocket flight to conclude that one of several 20-cm features was due to optically thick thermal bremsstrahlung associated with X-ray coronal loops. They noticed that the 20-cm radiation was concentrated at the tops of the X-ray loops and attributed this apparent concentration to absorption in a cool external plasma. However, such a concentration was not apparent in the data of Chiuderi-Drago et al. (1982).

Webb et al. (1986) concluded that complete X-ray loops could not be imaged at any single microwave wavelength, but they ignored the substantial indirect evidence of numerous observers who have associated loop-like 20-cm features with coronal loops. Their generalization was also based upon a comparison of a 7-hour 20-cm map with a single X-ray image made during a 5-min. rocket flight. (Comparisons of X-ray maps with 6 cm data are largely irrelevant, since the 6-cm radiation is usually due to a different radiation process in different parts of the active region.)

In this paper, we present comparisons of high-resolution 20-cm maps from the VLA with simultaneous X-ray images from the SMM-FCS. These comparisons are given in §II. In one instance, all of the X-ray emitting plasma was detected at 20 cm, and additional 20-cm emission was observed near sunspots where no X-ray radiation was detected. However, the 20-cm radiation was concentrated at the apex of the more extensive X-ray coronal loops of another active region. In §III, we discuss the absorption and radiation mechanisms for coronal loops at 20 cm. We next use X-ray measurements of electron temperature and electron density to place constraints on these mechanisms. The observed 20-cm features are then explained. Our results are summarized in §IV, where we also discuss the potential of future 20-cm (VLA) and soft X-ray (SMM-FCS) comparisons.

II. OBSERVATIONS

We have used the VLA and the SMM-FCS to observe solar active regions AR 4508 and AR 4532 on 1984 June 4 and 1984 July 8, respectively. The VLA was in the C configuration on June 4 and in the hybrid C-D configuration on July 8. In both instances, the signal wavelength was 20.7 cm (1446 MHz) and the bandwidths were 12.5 MHz. Active region AR 4508 was observed with the VLA between 1500 UT and 2300 UT on June 4; its position on the solar surface was 06° N and 57° E at 1300 UT on this day. Active region AR 4532 was observed between 1800 UT and 2300 UT on July 8; its position on the solar surface was 07° S and 18° E on this day. The Flat Crystal Spectrometer (FCS) observed six prominent soft X-ray lines: OV III at 18.9 A, Ne IX at 13.4 A, Mg XI at 9.2 A, Si XIII at 6.7 A, S XV at 5.0 A and Fe XXV at 1.9 A. The FCS observed AR 4508 and AR 4532 throughout the time the VLA was observing these regions.

The half-power beamwidth of the individual VLA antennae was about 30' at 20 cm wavelength, and the synthesized maps constructed from up to 325 interferometer pairs had beamwidths of 12.6" x 15.5" in the C configuration and 12.6" x 36.0" in the C-D configuration. The June 4 data were calibrated by 5 minute observations of the calibrator source PKS 0528 + 134 every 35 minutes, while the July 8 data were similarly calibrated with the source PKS 0742 + 103. The flux densities of PKS 0528 + 134 and PKS 0742 + 103 were 1.5 Jy and 3.3 Jy at 1446 MHz, respectively. The calibrated data for the entire observing period were used together with the standard CLEAN procedure to make synthesis maps of both the total intensity, I, and the circular polarization, or Stokes parameter, V. No solar bursts or flares were observed, and the synthesis maps therefore refer to the quiescent, or non-flaring, radio emission. There was no detectable circular polarization ($V/I < 15\%$) for both active regions, suggesting that they were both

optically thick to the extraordinary and ordinary modes of wave propagation at 20 cm.

The 14" collimated field of view of the FCS was rastered over a 7' x 7' field of view on June 4 and over a 4' x 4' field of view on July 8; in each case the pixel spacing was 10" x 10". X-ray images were obtained for each of the six spectral lines during the orbital day at a cadance of 410 s. All of the available data for each spectral line were then summed and averaged during each orbit to improve the statistical uncertainty on the count rate from each pixel. Significant emission was only detected from the three softest channels -O VIII, Ne IX and Mg XI. The peak formation temperatures for these lines are 3 x 10^6 K, 4 x 10^6 K and 7 x 10^6 K, respectively. The failure to detect emission in the harder, more energetic, channels indicates that the active regions were unperturbed by flaring activity during the periods of observation.

The XRP also produced a white-light image that showed the sunspots, making it possible to align the X-ray images with the sunspots to an accuracy of 10". The VLA maps of the total intensity, I, at 20 cm were aligned with Hα photographs of the same sunspots with a similar 10" accuracy. This enabled us to compare the soft X-ray and 20-cm data with the same field of view and angular scale.

The 20-cm radiation of AR 4508 is concentrated in the central regions of a more extensive system of X-ray loops (Figure 1). In this instance, the 20-cm radiation was aligned along the magnetic neutral line (Figure 2). There is a sharp drop in the intensity of the radio emission along the edges of the magnetic neutral line where there ought to be a sharp gradient in the magnetic field strength.

However, all of the X-ray emitting plasma of AR 4532 was detected at 20 cm, and additional 20-cm emission was observed near and above sunspots where no X-ray radiation was detected. Intense X-ray radiation and intense 20-cm radiation were

detected from coronal loops or arcades of loops that are connected with underlying sunspots (Figure 3). These loops were about 60" across or about 5 x 10^9 cm in linear extent. Both X-ray and 20-cm radiation were also emitted from regions of bright plage. In addition, Lang et al. (1986) presented simultaneous FCS-VLA data in which an entire system of X-ray loops was completely imaged at 20 cm.

Thus, the same coronal loops are often detected at both 20-cm and X-ray wavelengths, with extra information at 20 cm near and above sunspots. Of course, the 20-cm coronal loops can also be limited to a smaller volume than their X-ray counterparts, but our FCS-VLA comparisons and other VLA observations suggest that this is not usually the case. The claim by Webb et al. (1986) that complete X-ray loops may never be imaged at any microwave wavelength can no longer be justified. We will therefore now turn our attention to the absorption and radiation mechanisms that account for the 20 cm-coronal loops.

III. DISCUSSION

Because the microwave brightness temperature, T_B, of the quiescent coronal loops is nearly equal to the electron temperature, T_e, the quiescent radiation from 20-cm loops is most likely thermal. The two possible thermal radiation mechanisms at 20 cm wavelength are thermal bremsstrahlung, or free-free emission, and thermal gyroresonance radiation, or cyclotron emission. In order to identify the dominant thermal radiation mechanism at 20 cm wavelength, we will evaluate the electron temperture, T_e, and the electron density, N_e, using the X-ray radiation that is attributed to thermal bremsstrahlung alone.

As previously mentioned, the active regions were so quiescent that they were only detectable in the three softest X-ray channels (O VIII, Ne IX and Mg XI). Because the O VIII to Ne IX line intensity ratio is insensitive to temperature variations over the range typical of solar active regions, the ratios of the other two lines (O VIII to Mg XI and Ne IX to Mg XI) were used as temperature diagnostics. The temperatures inferred from the two ratios were averaged to obtain our estimate for the electron temperature.

An emission measure was inferred from the temperatures and the observed X-ray fluxes. The electron density was then calculated using a volume of 3×10^{27} cm^3, which equals the product of the FCS pixel area and a typical soft X-ray scale height of 3×10^9 cm.

The mean electron temperatures, T_e, and electron densities, N_e, for AR 4508 were determined for the areas marked A, B and C in Figure 4. These parameters are given in Table 1 together with the maximum observed brightness temperature, T_B, at 20 cm wavelength and the optical depth $\tau = T_B/T_e$. The mean T_e and N_e for AR 4532 were similarly inferred for the areas marked A, B, C, D, E and F in Figure 5; they are given in Table 2 together with the relevant T_B and τ.

The mean values for different areas were then combined to give average values of $T_e = 3.0 \pm 0.2 \times 10^6$ K and $N_e = 2.7 \pm 0.3 \times 10^9$ cm^{-3} for AR 4508 and $T_e = 3.0 \pm 0.1 \times 10^6$ K and $N_e = 2.4 \pm 0.4 \times 10^9$ cm^{-3} for AR 4532. Here the uncertainties correspond to the standard deviation of the line ratios. These values of T_e and N_e are typical values for quiescent coronal loops in active regions.

Within the uncertainties, the observed loops were isothermal. They also all had optical depths $\tau < 1$ (optically thin). We will therefore evaluate the loop width or thickness, W, that would give rise to optically-thin thermal bremsstrahlung at our observing frequency of $\nu = 1446$ MHz (20.75 cm). According to Lang (1980):

$$W < \frac{102\ \tau_{f-f} \nu^2\ T_e^{3/2}}{N_e^2\ \ln\ (4.7 \times 10^{10}\ T_e/\nu)}\ , \qquad (1)$$

or

$$W < \frac{2.13 \times 10^{20}\ \tau_{f-f}\ T_e^{3/2}}{N_e^2\ \ln\ (32.5\ T_e)}\ \text{cm},$$

where τ_{f-f} is the optical depth for bremsstrahlung. The N_e and T_e obtained from the X-ray observations were substituted into equation (1) to provide the widths, W, given in Tables 1 and 2. The average values of W for the two active regions are $W < 4 \times 10^9$ cm and $W < 5 \times 10^9$ cm, which are certainly plausible.

However, we will next evaluate the optical depth τ_{g-r} for gyroresonance absorption by using the equation (Zheleznyakov 1970)

$$\tau_{g-r} = 0.052\ \frac{n^{2n}}{2^{n+1} n!}\ \frac{N_e}{\nu}\ (1.7 \times 10^{-10}\ T_e)^{n-1} L_H\ (1 \pm \cos\alpha)^2\ \sin^{2n-2}\ \alpha \qquad (2)$$

where the magnetic scale length L_H has typical values of $L_H \sim 1 \times 10^9$ cm, the angle between the line of sight and the direction of the magnetic field lines is α, and our observing frequency $\nu = 1446$ MHz and the harmonic n is related to ν through the relation

$$\nu = 2.8 \times 10^6 \text{ nH Hz}, \tag{3}$$

where the magnetic field strength is H. For typical values of H ~ 130 G at the apex of coronal loops (Willson 1985; Lang et al. 1986), we have n = 4. Then, collecting terms in equation (2), we have for $\alpha = 90°$ and n = 4:

$$\tau_{g-r} = 3.1 \, N_e \, (1.7 \times 10^{-10} \, T_e)^3.$$

Our average X-ray values of $N_e \sim 2.5 \times 10^9$ cm^{-3} and $T_e \sim 3 \times 10^6$ K give $\tau_{g-r} \sim 1.0$ for n = 4.

Thus, we expect thermal gyroresonance radiation to be optically thick for plausible loop widths and magnetic scale lengths. This is consistent with the lack of any detectable circular polarization at 20 cm. The observed brightness temperature, T_B, at 20 cm wavelength should therefore be equal to the electron temperature with $T_B = T_e$, but the values of T_B are about five times smaller than T_e. To resolve this paradox, we call attention to an idea first proposed by Holman (1986).

To explain the restriction of one 20-cm loop to the apex of an X-ray loop, Holman argued that cooler material with $T_e \sim 10^5$ K exists either as a sheath around the loops or as part of an external medium. The 20-cm radiation emitted by the X-ray loops will be partly absorbed in the cooler, higher plasma, thereby reducing its brightness temperature. The cooler, higher material would, however, be invisible in X-rays because of its low temperature and relatively small emission measure.

If the cool plasma is part of an external medium that is more extensive than the X-ray loops, then we would expect the observed 20-cm loops to be co-spatial with the X-ray ones, but with a lowered brightness temperature. This is in fact observed for AR 4532. When the cool plasma is part of a sheath around the X-ray loops, then the line of sight through the low-temperature plasma will be greatest at the loop edges and footpoints, and the observed 20-cm emission will be concentrated at the apexes of the X-ray coronal loops. This is observed for AR 4508.

What about the bright 20 cm radiation near and above sunspots? There is no detectable X-ray radiation in these regions, and this can be attributed to a low electron density, N_e. Because the optical depth for free-free absorption scales with N_e^2 while that for gyroresonance absorption scales with N_e, the low electron density favors gyroresonance absorption. The high magnetic field strength above sunspots also favors this process. We therefore attribute the 20-cm radiation near and above sunspots to thermal gyroresonance radiation.

IV. SUMMARY

The quiescent, or non-flaring, X-ray radiation of solar active regions is attributed to thermal bremsstrahlung, but the quiescent microwave radiation may be due to either thermal bremsstrahlung or thermal gyroresonant radiation. In the introduction, we reviewed evidence for thermal gyroresonance radiation at 6 cm in coronal regions above sunspots. This evidence includes comparisons of 6 cm VLA maps with simultaneous soft X-ray data, as well as the detection of highly circularly-polarized horseshoe-shaped structures above sunspots at 6 cm. Bright 6-cm sources are not expected to coincide with bright soft X-ray sources because their different radiation mechanisms dominate different parts of solar active regions.

Although the thermal bremsstrahlung of coronal loops is usually optically thin at 6 cm, it might become optically thick at the longer 20-cm wavelength where loop-like coronal structures are observed. These 20-cm coronal loops stretch between regions of opposite magnetic polarity in the underlying photosphere, and the temperatures, sizes and shapes of the 20-cm coronal loops resemble those of soft X-ray coronal loops.

In this paper we have compared high-resolution 20-cm maps (VLA) with simultaneous high-resolution X-ray images (SMM-FCS) of two active regions. The X-ray coronal loops in AR 4532 were completely imaged at 20 cm, while the 20-cm emission of AR 4508 was concentrated along the magnetic neutral line within more extended X-ray loops. The X-ray data were used to infer an average $T_e = 3.0 \pm 0.2 \times 10^6$ K and an average $N_e = 2.7 \pm 0.3 \times 10^9$ cm^{-3} for AR 4532 and the average $T_e = 3.0 \pm 0.1 \times 10^6$ K and $N_e = 2.4 \pm 0.4 \times 10^9$ cm^{-3} for AR 4508.

The microwave brightness temperatures, T_B, at 20 cm were always less than the average electron temperature, with optical depths $\tau = T_e/T_B$ of $0.2 < \tau < 0.5$. The X-ray values of T_e and N_e indicate that thermal bremsstrahlung ought to be optically thin at 20 cm for plausible loop widths, but the thermal gyroresonance radiation can be optically thick at 20 cm for plausible magnetic field strengths and scale heights. Optically thick radiation is also consistent with the lack of detectable circular polarization at 20 cm. Thermal gyroresonance radiation must account for the intense 20-cm radiation near and above sunspots where no X-ray radiation is detected.

The unexpectedly low values of T_B can be explained if the X-ray emitting coronal loops lie beneath a higher, cooler plasma. The hot, dense plasma in the X-ray coronal loops would emit optically thick radiation at 20 cm wavelength, but the brightness temperature of this radiation would be reduced during subsequent

propagation through the cooler, absorbing plasma. The observations of AR 4532 can be explained if the cooler plasma extends across and beyond thee X-ray loops, while the AR 4508 results might be explained by the presence of a cool sheath around the X-ray loops. The cooler material would not be detected at X-ray wavelengths because of its low temperature and relatively small emission measure.

The results given in this paper indicate that the structure and dominant radiation mechanisms in the low corona are much more complex and inhomogeneous that was previously thought. Systems of coronal loops within a single active region apparently have different temperatures and different radiation mechanisms that can only be detected by observations at both X-ray and 20cm wavelength. Future comparisons of high-resolution images at these two wavelengths will lead to detailed information about the plasma and magnetic structure of the low solar corona. Physical parameters such as electron temperature, electron density and magnetic field strength can be specified, and the detailed variation of these parameters within the coronal atmosphere can be determined. Such information will provide important constraints on theories and models of coronal loops as well as general theories for the structure and heating of solar active regions.

Radio astronomical studies of the Sun at Tufts University are supported under grant AFOSR-83-0019 with the Air Force Office of Scientific Research and Contract N00014-86-K-0068 with the Office of Navel Research (ONR). Simultaneous VLA and SMM-FCS observations of the Sun are supported by NASA grant NAG 5-501. K.L.S. and K.T.S. are supported by NASA contract NAS 5-23758 and the Lockheed Independent Research Program. The XRP was built by a consortium of three groups: Lockheed Palo Alto Research Laboratory, Mullard Space Science Laboratory, and the Rutherford and Appleton Laboratories. The VLA is operated by Associated Universities Inc., under contract with the National Science Foundation.

REFERENCES

Alissandrakis, C.E., and Kundu, M.R. 1982, Ap. J. (Letters) 253, L49.

Chiuderi-Drago, F., Bandiera, R., Falciani, R., Antonucci, E., Lang, K.R., Willson, R.F., Shibasaki, K. and Slottje, C. 1982, Solar Phys. 80, 71.

Dulk, G.A., and Gary, D.E. 1983, Astr. Ap. 124, 103.

Gary, D.E., and Hurford, G.J. 1986, "Multi-Frequency Observations of a Solar Active Region During a Partial Eclipse", B.B.S.O. 0259, submitted to Ap. J.

Gel'friekh, G.B., and Lubyshev, B.I. 1979, Sov. Astron. A.J. 23, 316.

Holman, G.D. 1986, "High-Spatial-Resolution Microwave and Related Observations as Diagnostics of Coronal Loops", to be published in Coronal And Prominence Plasmas.

Kundu, M.R., and Lang, K.R. 1985, Science 228, 9.

Kundu, M.R., Schmahl, E.J., and Gerassimenko, M. 1980, Astr. Ap. 82, 265.

Lang, K.R. 1980, Astrophysical Formulae (2nd Ed. New York: Springer Verlag).

Lang, K.R., and Willson, R.F. 1982, Ap. J. (Letters) 255, L111.

Lang, K.R., and Willson, R.F. 1983, Adv. Space Res. 2, No. 11, 91.

Lang, K.R., and Willson, R.F. 1984, Adv. Space Res. 4, No. 7, 105.

Lang, K.R., Willson, R.F., and Gaizauskas, V. 1983, Ap. J. 267, 455.

Lang, K.R., Willson, R.F., and Rayrole, J. 1982 Ap. J. 258, 384.

Lang, K.R., Willson, R.F., Smith, K.L. and Strong, K.T. 1986, "Solar Active Region Physical Parameters Inferred From A Thermal Cyclotron Line and Soft X-ray Spectral Lines", submitted to Ap. J.

McConnell, D., and Kundu, M.R. 1983, Ap. J. 269, 698.

Pallavicini, R., Sakurai, T., and Vaiana, G.S. 1981, Astr. Ap. 98, 316.

Schmahl, E.J., Kundu, M.R., Strong, K.T., Bentley, R.D., Smith, J.B., and Krall, K.R., 1982, Solar Phys. 80, 233.

REFERENCES - Continued

Shevgaonkar, R.K, and Kundu, M.R. 1984, Ap. J. 283, 413

Shibasaki, K., Chiuderi-Drago, F., Melozzi, M., Slottje, C., and Antonucci, E. 1983, Solar Phys. 89, 307.

Strong, K.T., Alissadrakis, C.E., and Kundu, M.R. 1984, Ap. J. 277, 865.

Vaiana, G.S., and Rosner, R. 1978, Ann. Rev. Astron. Ap. 16, 393.

Webb, D.F., Davis, J.M., Kundu, M.R., and Velusamy, T. 1983, Solar Phys. 85, 267.

Webb, D.F., Holman G.D., Davis, J.M., Kundu, M.R., and Shevgaonkar, R.K. 1986, "The Plasma and Magnetic Field Properties of Coronal Loops Observed at High Spatial Resolution", submitted to Ap. J.

Willson, R.F. 1985, Ap. J. 298, 911.

Zheleznyakov, V.V. 1970, Radio Emission of the Sun and Planets (New York: Pergamon Press), p. 454.

KENNETH R. LANG and ROBERT F. WILLSON:
Department of Physics and Astronomy
Robinson Hall
Tufts University
Medford, MA 02155

KERMIT L. SMITH and KEITH T. STRONG
Code 602.6
Bldg. 7-XRP
Goddard Space Flight Center
Greenbelt, MD 20771

Table 1. The mean electron temperature, T_e, mean electron density, N_e, maximum brightness temperature, T_B, at 20 cm wavelength, optical depth, τ, and the inferred loop width or thickness, W, for the areas of AR 4508 marked A, B, and C in Figure 4.

Region	T_e (10^6K)	N_e (10^9cm-3)	T_B (10^6K)	τ	W (10^9cm)
A	3.3	2.7	0.8	0.27	3
B	2.9	3.0	1.7	0.88	6
C	3.0	2.8	1.0	0.41	3
Average	3.1	2.8	1.2	0.52	4

Table 2. The mean electron temperature, T_e, mean electron density, N_e, maximum brightness temperature, T_B, optical depth, τ, and inferred loop width or thickness, W, for the areas of AR 4532 marked A, B, C, D, E, and F in Figure 5.

Region	T_e (10^6K)	N_e (10^9cm^{-3})	T_B (10^6K)	τ	W (10^9cm)
A	2.9	2.4	1.3	0.60	6
B	2.8	2.1	0.8	0.34	4
C	3.1	2.1	0.8	0.30	4
D	3.3	3.0	1.4	0.55	4
E	2.7	2.1	1.4	0.73	8
F	2.7	2.1	0.7	0.30	4
Average	2.9	2.3	1.1	0.47	5

FIGURE LEGENDS

Fig. 1. A comparison of a 20 cm VLA synthesis map of AR 4508 with SMM-FCS images in the O VIII (18.9 A) and Mg XI (9.2 A) lines on June 4 1984. The field of view of all three images is the same, and the angular scale can be inferred from the 60" spacing between fiducial marks on the axes. The contours of the 20-cm map mark levels of equal brightness temperature corresponding to 0.4, 0.5, 0.6 ... 1.0 times the maximum brightness temperature of 1.7×10^6 K. The contours of the O VIII image correspond to 4, 8 and 15 counts s^{-1} above a background level of 10 counts s^{-1} with a maximum signal of 20 counts s^{-1}. The contours of the Mg XI image are the same as those of O VIII with a background level of 5 counts s^{-1} and with a maximum signal of 15 counts s^{-1}.

Fig. 2. The 20 cm contours of equal brightness temperature (solid black lines) are superposed on a Kitt Peak National Observatory (KPNO) magnetogram of AR 4508 on 1984 June 4. The radio emission is concentrated along the magnetic neutral line that separates regions of negative (black) and positive (white) magnetic polarity. Sharp magnetic field gradients may exist along the neutral line. The KPNO magnetogram was kindly provided by Jack Harvey of the National Solar Observatory.

Fig. 3. A comparison of soft X-ray (SMM-FCS-left), Hα (SOON-middle) and 20 cm (VLA-right) images of AR 4532 on 1984 July 8. The field of view of all three images is the same, and the angular scale can be inferred from the 120" spacing between the fiducial marks on the axes. The contours of the 20 cm map mark levels of equal brightness temperature corresponding 0.4, 0.5, 0.6 ... 1.0 times the maximum brightness temperature of 1.4×10^6 K. The soft X-ray data were

taken in the O VIII line (18.9 A) with contours corresponding to 4, 8 and 15 counts s^{-1} above a background level of 10 counts s^{-1} with a maximum signal of 20 counts s^{-1}. Here the sunspots are denoted by small black dots with a circle around them.

Fig. 4. A soft X-ray map of AR 4508 taken in the Mg XI line (9.2 A) with contours corresponding to 4, 8 and 15 counts s^{-1}. The ratios of the O VIII and Mg XI line intensities were used to determine the mean electron temperatures in the regions marked A, B and C. These temperatures, the mean electron density, 20-cm brightness temperature, optical depth and loop width are given in Table 1. There is no detectable soft X-ray radiation in the vicinity of the sunspots marked E and F, but these regions are associated with intense radiation at 20-cm wavelength (also see Figure 3).

Fig. 5. A soft X-ray map of AR 4532 taken in the O VIII line (18.9 A) with contours corresponding to 4, 8 and 15 counts s^{-1}. The ratios of the O VIII and Mg XI line intensities were used to determine the mean electron temperature in the regions marked A, B, C, D, E and F. These temperatures, the mean electron density, 20-cm brightness temperature, optical depth and loop width are given in Table 2.

Figure 1.

Figure 3.

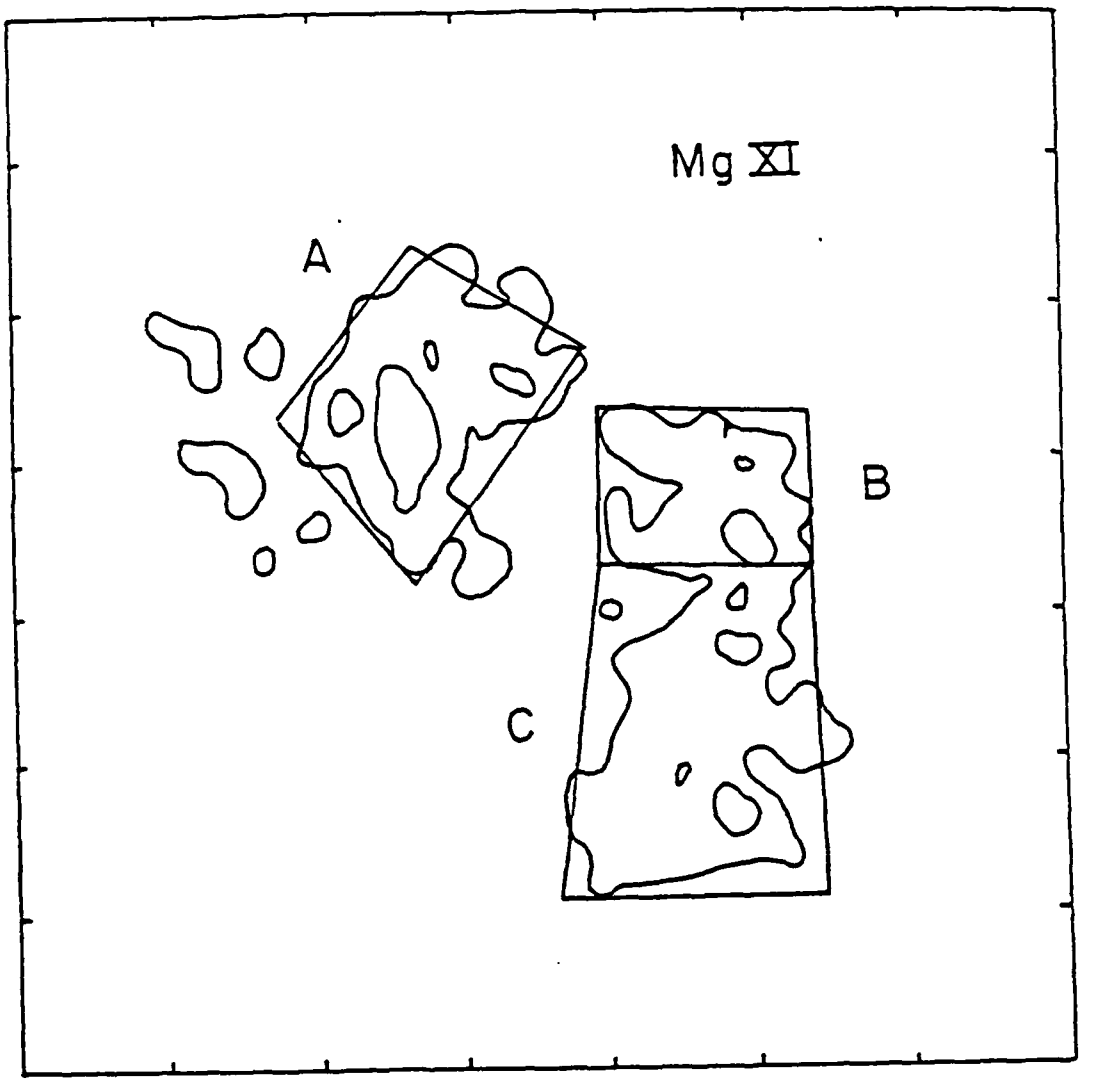

Figure 4.

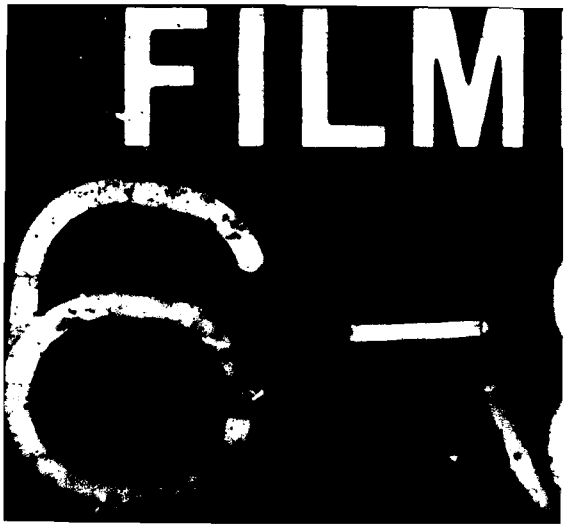
FILM